Supporting Information

Cobalt single-atom decorated nickel thiophosphate nanosheets for overall water splitting

Jian Zhang,*[a,b] Niannian Zhou,[a] Ming Du,[b] Yonghua Li,[b] Yan Cui,[c] Xing'ao Li,*[a,b] Xinbao Zhu[d] and Wei Huang[b,e]

a. New Energy Technology Engineering Lab of Jiangsu Province, College of Science, Nanjing University of Posts & Tele-communications (NUPT), Nanjing 210023, P. R. China. E-mail: iamjzhang@njupt.edu.cn; lxahbmy@126.com

b. State Key Laboratory of Organic Electronics and Information Displays and Institute of Advanced Materials (IAM), Nanjing University of Posts and Telecommunications (NUPT), Nanjing 210023, Jiangsu, P. R. China

c. Key Laboratory of Broadband Wireless Communication and Sensor Network Technology, Ministry of Education, Nanjing University of Posts and Telecommunications, Nanjing 210023, P. R. China

d. College of Chemical Engineering, Nanjing Forestry University, Nanjing 210037, P. R. China

e. Institute of Flexible Electronics (IFE), Northwestern Polytechnical University (NPU), Xi'an 710072, P. R. China

1. Experimental section

1.1 Synthesis of bulk and monolayered $NiPS_3$ crystals.

Bulk $NiPS_3$ were obtained through heating catalyst powder in vacuum. In short, 1.5 g of Ni, P and S powders with a stoichiometric mole ratio of 1 : 1 : 3 were fully mixed and ground in glove box, followed by sealing in an evacuated quartz tube under vacuum. Subsequently, the sealed tube was placed in a two-zone furnace. The temperature in the reaction and growth zone were programmed to 750 °C and 680 °C for 6 days with a heating rate of 1.5 °C min^{-1} to assemble bulk $NiPS_3$ crystals. Finally, the two-zone furnace was cooled naturally to room temperature, and the solid powder was washed with carbon disulfide to obtain the bulk $NiPS_3$ crystals.

Monolayered $NiPS_3$ nanocrystals were prepared via an exfoliation process. Typically, bulk $NiPS_3$ powder (30 mg) was added into 100 mL of absolute ethylalcohol and then it was exfoliated by ultrasonication for 48 h. After that, the mixed solution was centrifuged at 3000 rpm, the residual bulk sample can be removed; afterwards the remaining sample was centrifuged again at 13,000 rpm. Finally, the moist solid powder was dispersed again in water and lyophilized to get the exfoliated $NiPS_3$.

1.2 Synthesis of Co nanodisks.

Co nanodisks were synthesized using standard air-free procedures.[1] In a typical synthesis, 0.1 g of trioctylphosphine oxide (TOPO, Technical Grade, Sigma Aldrich) was degassed with argon (High purity) for 20 min in a three-neck flask, followed by the introduction of 15 mL of anhydrous odichloride benzene (DCB, Technical Grade,

Sigma Aldric) and 0.1 mL of oleylamine (OA, Technical Grade, Sigma Aldric) under argon, heating to reflux (182 °C) and then rapidly injecting 0.54 g of cobalt carbonyl ($Co_2(CO)_8$, Co content ≥90%, Sigma Aldrich) containing 2% hexane diluted in 3 mL of DCB (precursor solution). After 10 min, the reaction was stopped by quenching in an ice water bath. The final products were processed by extracting the solution, washing several times with water and methanol to remove the possible ions and organic component, and finally suspending in argon-saturated water for measurement.

1.3 Synthesis of Co nanodisks/$NiPS_3$ (Co@$NiPS_3$) nanocomposites.

The Co nanodisks and $NiPS_3$ solution with an appropriate mass ratio were mixed together in a 20 mL bottle. The reaction system was degassed with argon for 30 min. Then, it was ultrasonically treated for 30 h in a thermostat reaction system with a constant temperature of 5 °C, power of 800W and frequency of 40 KHz. The final product was collected by extraction from the solution, washed with water several times, and finally suspended in argon-saturated water for measurement.

1.4 Synthesis of single-atom Co on $NiPS_3$ (SA Co $NiPS_3$).

The Co@$NiPS_3$ nanocomposites solution was drop casted onto a carbon fiber paper electrode. Then, the electrode was immersed in a 0.5 M H_2SO_4 solution, and the electrochemical leaching between 0.1 V to -0.3 V was performed for 200 cycles. The electrode was then dipped into an ethanol solution and sonicated for 30 min to peel the sample. The suspension was centrifuged at 11,000 rpm and lyophilized to get the final samples.

1.5 Materials characterization.

The morphologies of the samples were characterized by TEM (JEM-120F) and EDS (JEOL JED-2300 Analysis Station). STEM images were taken on a JEM-ARM200F TEM operated at 200 kV, equipped with a high angle annular dark field (HAADF) detector, while compositional maps were obtained with EDS using four large solid-angle symmetrical Si drift detectors, and the attainable resolution of the probe defined by the spherical-aberration coefficient of 78 pm, illumination semi-angle of 25 mrad and probe current of 100 pA. X-ray photoelectron spectroscopy (XPS) were acquired on an ESCALAB MK II with Mg Kα as the excitation source. Atomic force microscopy (AFM) on a Vecco Multimode using the tapping mode. The BET surface area was measured using the nitrogen gas adsorption-desorption method (TriStar II 3020) at 77 K. XRD measurements were carried out on a BRUKER D8 Advance X-diffractometer with Cu Kα radiation. Raman spectra were recorded on a Raman spectroscopy was performed with a laser micro-Raman spectrometer (Renishaw in Via, 532 nm excitation wavelength). Inductively coupled plasma-atomic emission spectrometry (ICP-AES) analysis was performed on a Thermo ICAP-6300 instrument (USA). XANES/EXAFS: 100 mg of sample was first ground into fine powder using a mortar and pestle before being pressed into a 10 mm pellet. Measurements were carried out at Singapore Synchrotron Light Source (SSLS), X-ray Absorption Fine structure for catalysis (XAFCA) beamline.[2] Data analysis and simulation were carried out on Athena, Artemis, and Hephaestus (Version 0.9.23).[3]

1.6 Electrochemical measurements.

Electrochemical measurements were carried out in 0.5 M H_2SO_4 electrolyte degassed

by nitrogen in a standard three electrode system on a CHI 660E electrochemical workstation (Shanghai, Chenhua Co., China) in which the working electrode was prepared by loading the ink containing 30 μg of the catalyst onto a glassy carbon rotating disk electrode (RDE). The high-purity graphite rod (99.999%) was used as the counter electrodes, and Ag/AgCl (3.5 M KCl electrolyte solution inside) was used as the reference electrode. Before testing, the electrolyte was bubbled with Ar for 0.5 h. During electrochemical experiments, RDE electrode was constantly rotating at 1600 rpm to remove the interference of the as-produced gas. The polarization curves were all corrected by iR-compensation (95%) to offset the interference of the Ohmic resistance. The electrochemical surface area was determined by cyclic voltammetry (CV) scans at different scan rates. The electrochemical impedance spectroscopy (EIS) response was performed at a frequency range from 0.01 Hz to 100 kHz with an amplitude of 5 mV.

To evaluate the electrocatalytic performance for overall water splitting in alkaline solutions, the catalyst dispersed in isopropanol and Nafion (5.0 wt%) was coated on two clean Ni foam pieces with the size about 1.0 × 2.0 cm^2. The loading amount of the electrocatalyst is 2.0 mg cm^{-2}. The as-fabricated electrodes were used as both cathode and anode. The alkaline electrolyzer was constructed using a two-electrode setup in a simple glass beaker containing 1.0 M KOH. The cathode was used as it is, while the anode was activated by 50 cyclic voltammetric scans (from 1.1 to 1.8 V). Linear Sweep Voltammetry (LSV) tests were carried out in a potential window of 1.0-2.0 V at a scan rate of 5.0 mV s^{-1} under continuous stirring. The galvanostatic

experiment was performed to test the stability of the electrolyzer at constant voltage.

1.7 Density Function Theory (DFT) calculations.

All models were calculated by Vienna *Ab initio* Simulation Package (VASP) using DFT[4] via generalized gradient approximation (GGA) Perdew-Burke-Ernzerhof (PBE) exchange-correlation functional.[5] Moreover, the projector-augmented-wave (PAW)[6] method was applied for the pseudopotentials. The energy cutoff for the plane wave basis expansion was set to 500 eV. The force and energy convergence criterions were set as 0.02 eV/Å and 10^{-4} eV, respectively. Monkhorst-Pack k-point sampling with k-point setting of 3*3*1 were applied for all calculations. The intermediate adsorbed on the (001) plane has a relatively stable structure, so the (001) plane were used to build the adsorption model here.[7] The structure of single Co atom coordinated with three sulfur atoms is selected as the optimized model of SA Co $NiPS_3$ for further investigation due to its much lower formation energy. The formation energy (E_f) for both cases has also been calculated to evaluate their structural stability, which is calculated as: $E_f = E_t - E_v - E_i$, where E_t is the total energy for $NiPS_3$ with substituted or absorbed Co atoms, E_v is the energy for $NiPS_3$ with one Ni vacancy in the substitutional case or for perfect $NiPS_3$ in the absorbed case, and E_i is the energy of single Co atom.

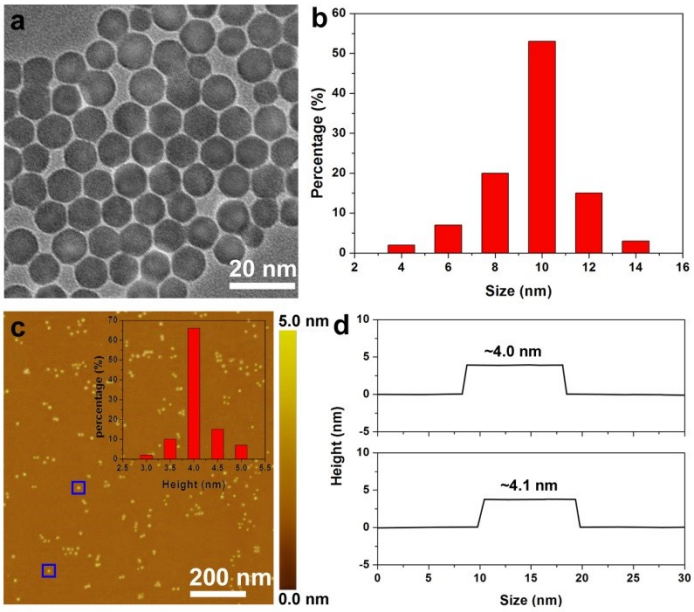

Figure S1. Characterization of the Co nanodisks. TEM image (a) and the size distribution (b) of Co nanodisks. (c) AFM image of Co nanodisks. Inset of (c) shows the average thickness of Co nanodisks and the corresponding height profiles (d).

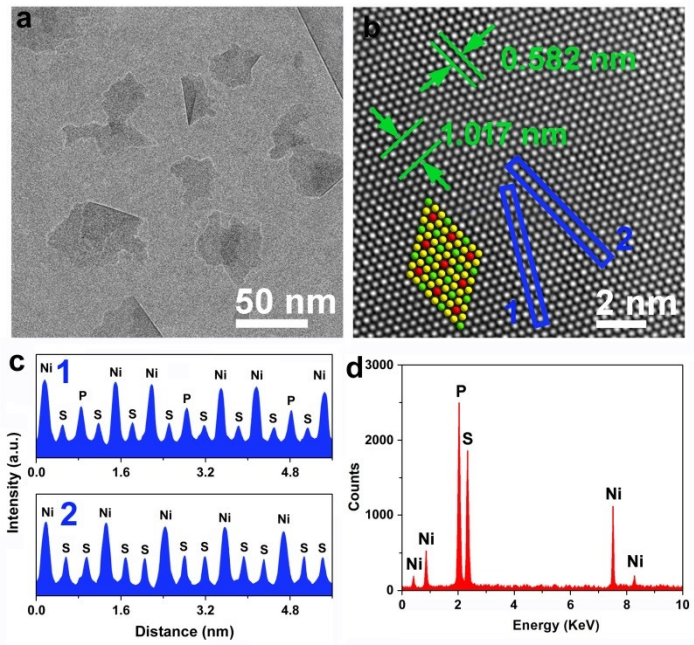

Figure S2. TEM (a) and HRTEM (b) images together with the line profiles (c) extracted from the areas marked with blue rectangles (b) of monolayered $NiPS_3$. (d) Energy-X-ray spectra of $NiPS_3$.

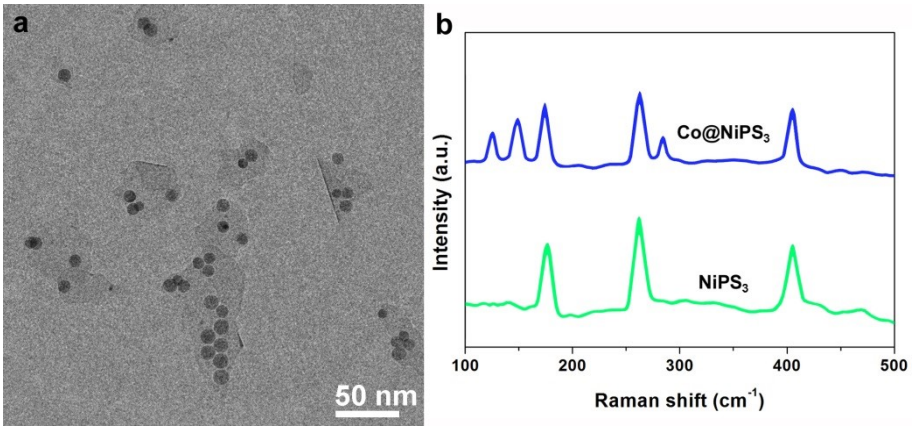

Figure S3. (a) TEM image of $Co@NiPS_3$. (b) Raman spectra of $NiPS_3$ and $Co@NiPS_3$.

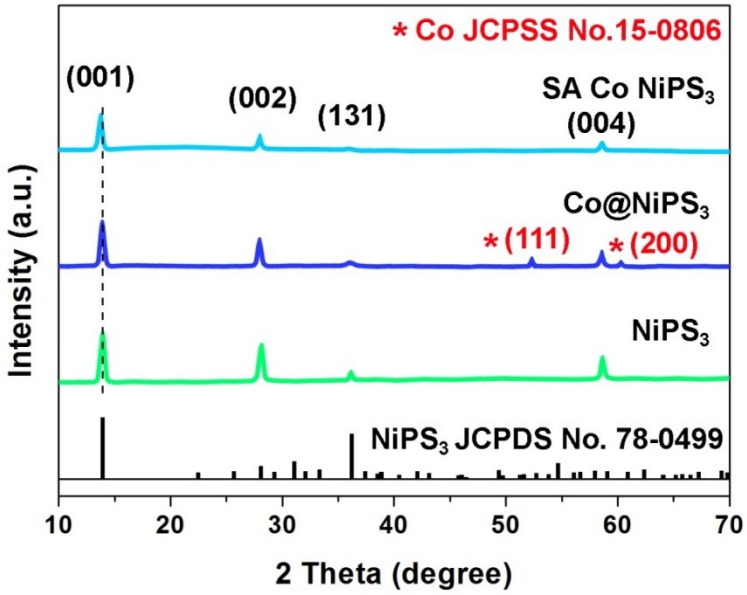

Figure S4. XRD patterns of pristine $NiPS_3$, $Co@NiPS_3$, and SA Co $NiPS_3$.

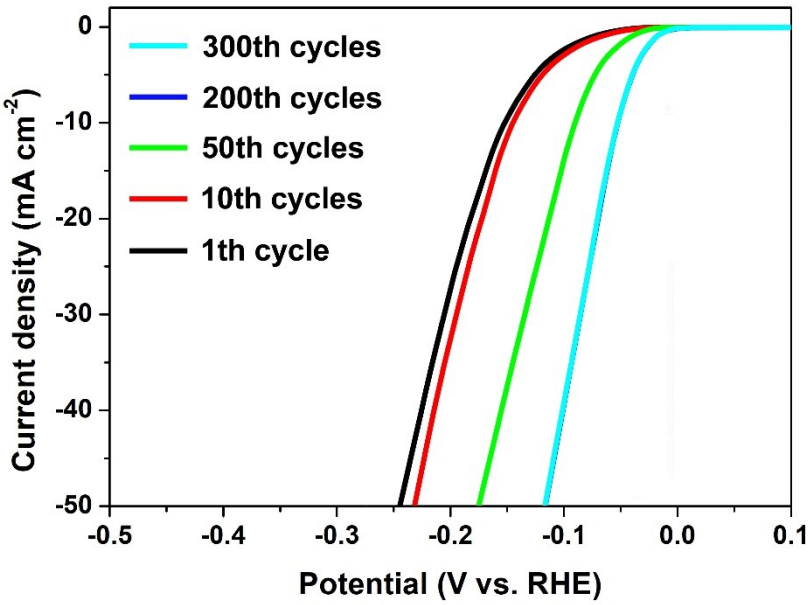

Figure S5. HER polarization curves of the Co@$NiPS_3$ with different cycles between 0.1 and -0.3 V at a rate of 50 $mV \cdot s^{-1}$.

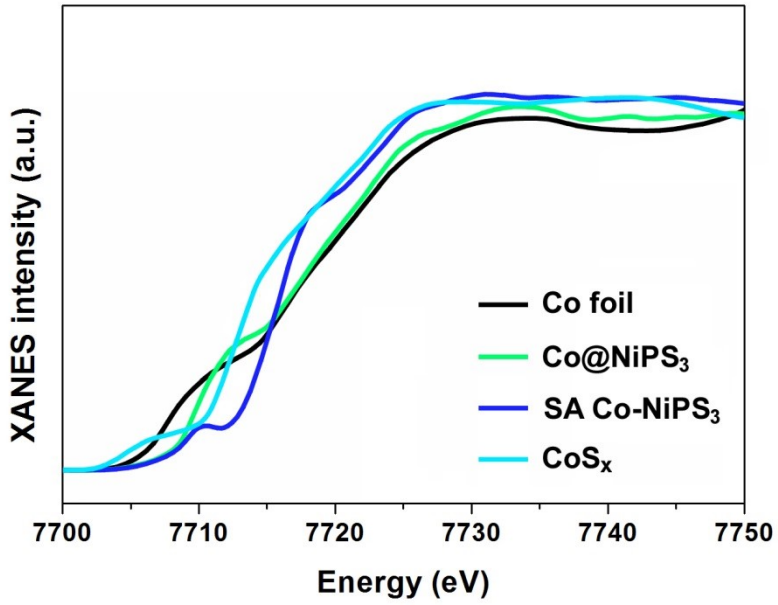

Figure S6. Co K-edge XANES spectra of Co foil, CoS_x, Co@$NiPS_3$, and SA Co $NiPS_3$.

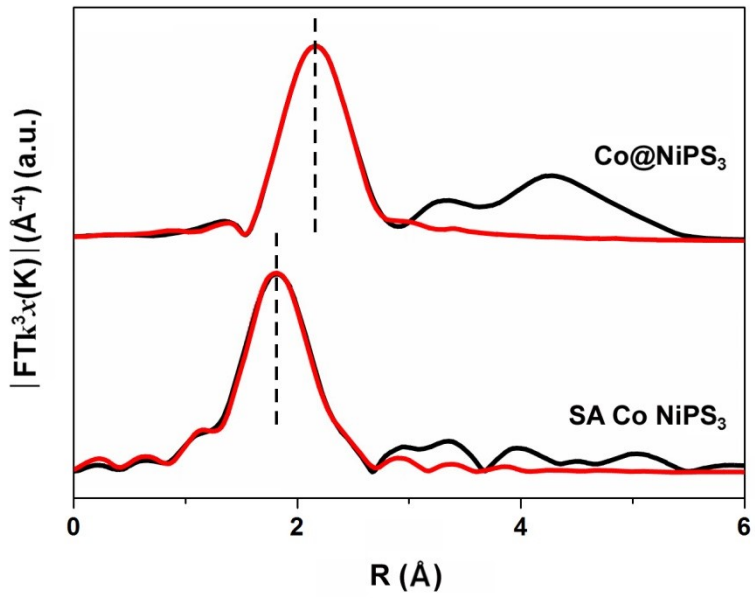

Figure S7. Fourier-transformed magnitude of Co K-edge EXAFS spectra in R space for Co@$NiPS_3$ and SA Co $NiPS_3$.

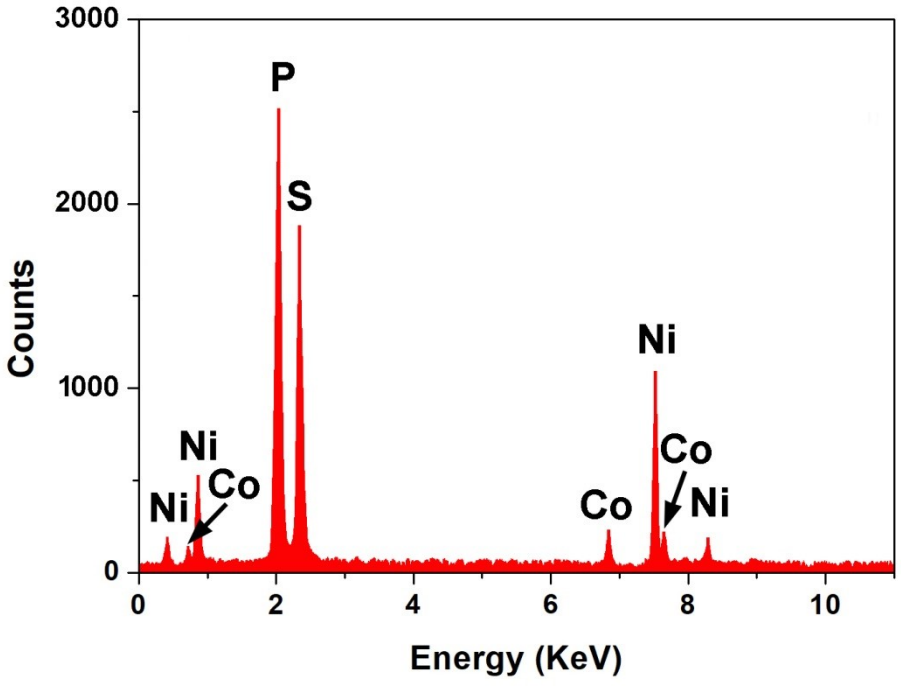

Figure S8. Energy-X-ray spectra of SA Co $NiPS_3$.

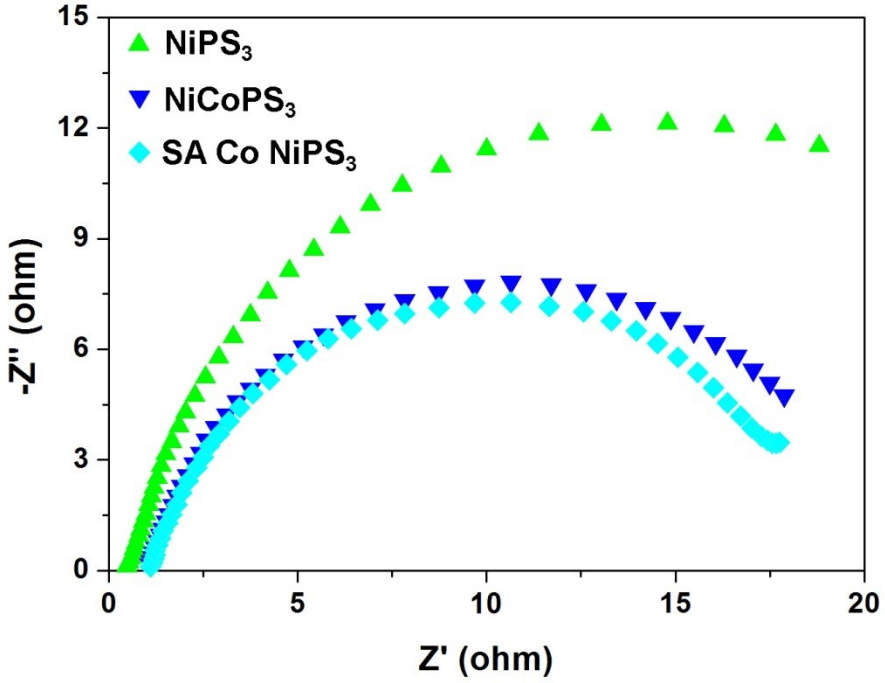

Figure S9. Electrochemical impedance spectra (EIS) of $NiPS_3$, Co@$NiPS_3$ and SA Co $NiPS_3$.

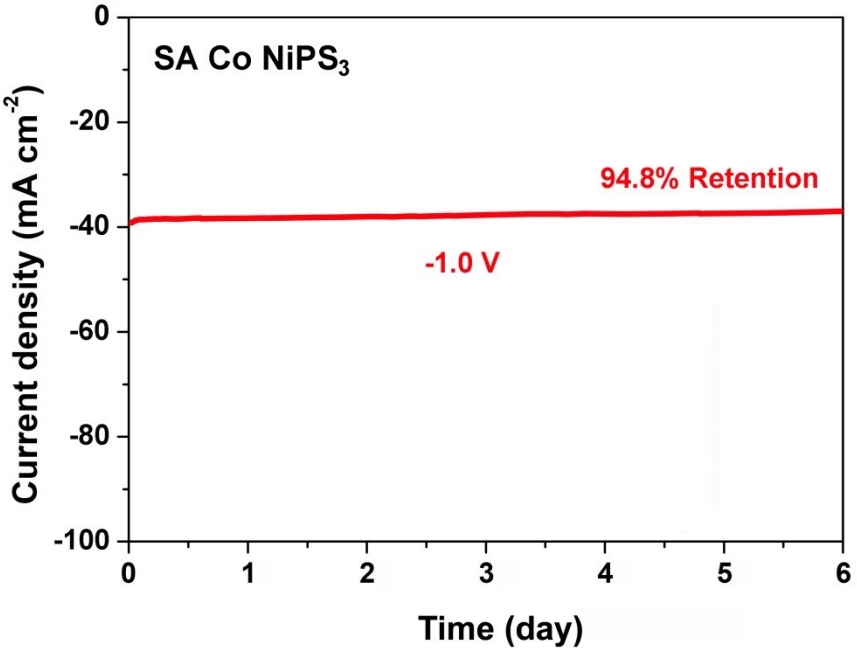

Figure S10. The HER durability tests of the SA Co $NiPS_3$ at -1.0 V applied potential.

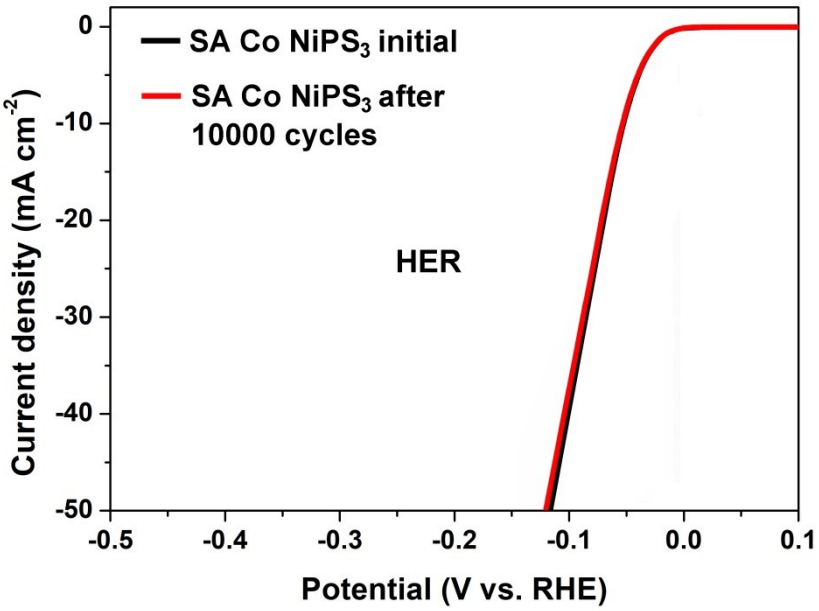

Figure S11. Polarization curves of the SA Co $NiPS_3$ recorded before and after 10000 cycles.

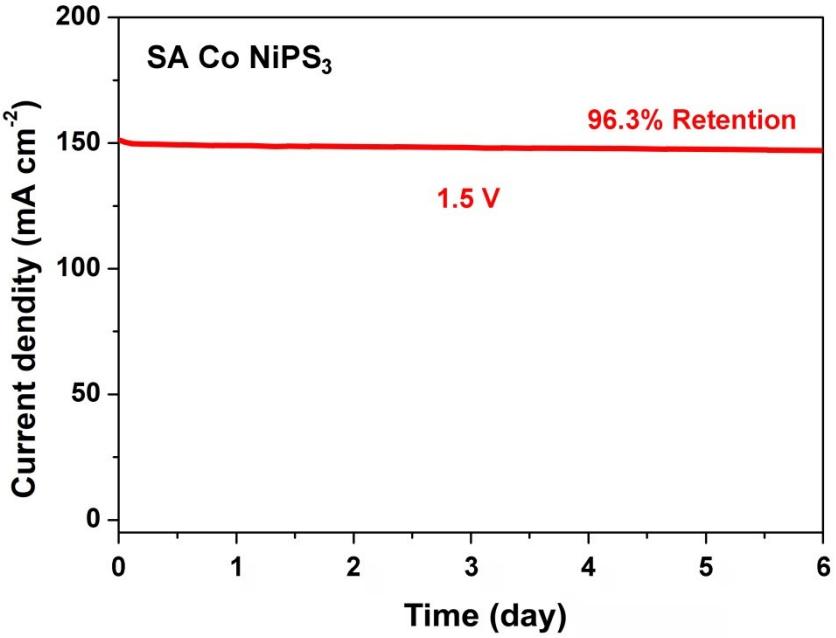

Figure S12. The OER durability tests of the SA Co $NiPS_3$ at 1.5 V applied potential.

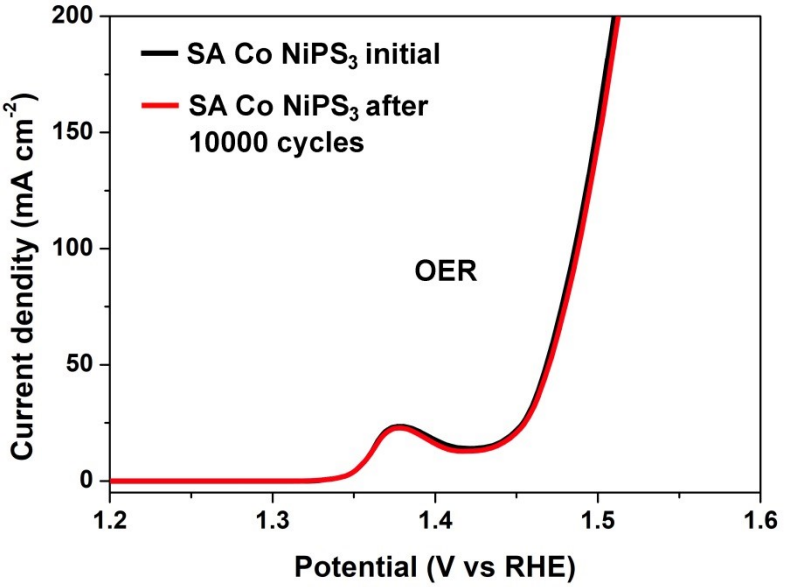

Figure S13. Polarization curves of the SA Co $NiPS_3$ recorded before and after 10000 cycles.

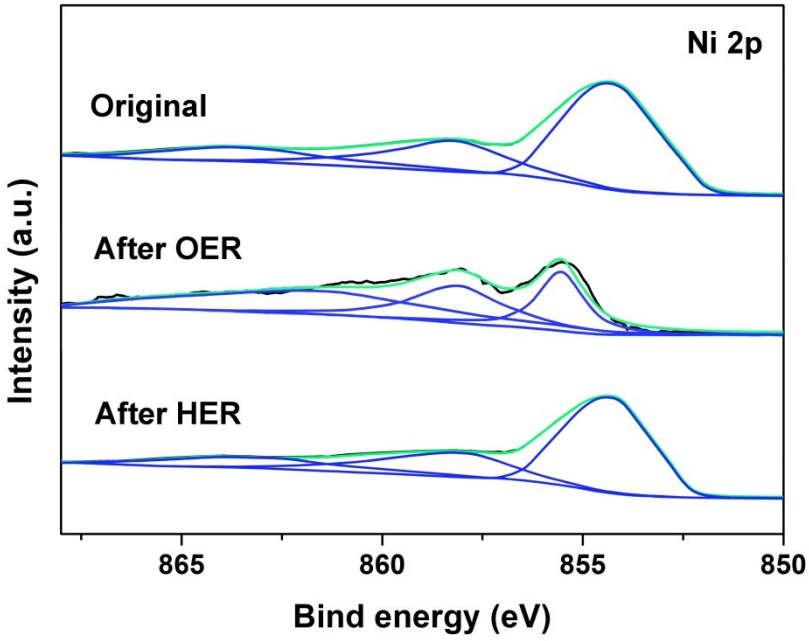

Figure S14. High-resolution XPS spectra for Ni 2p of SA Co $NiPS_3$ (original, after HER, and after OER).

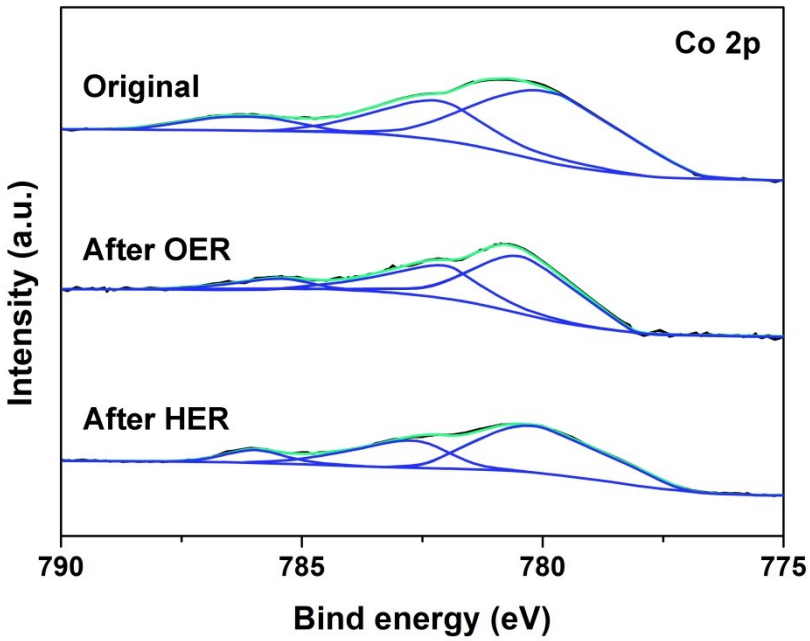

Figure S15. High-resolution XPS spectra for Co 2p of SA Co $NiPS_3$ (original, after HER, and after OER).

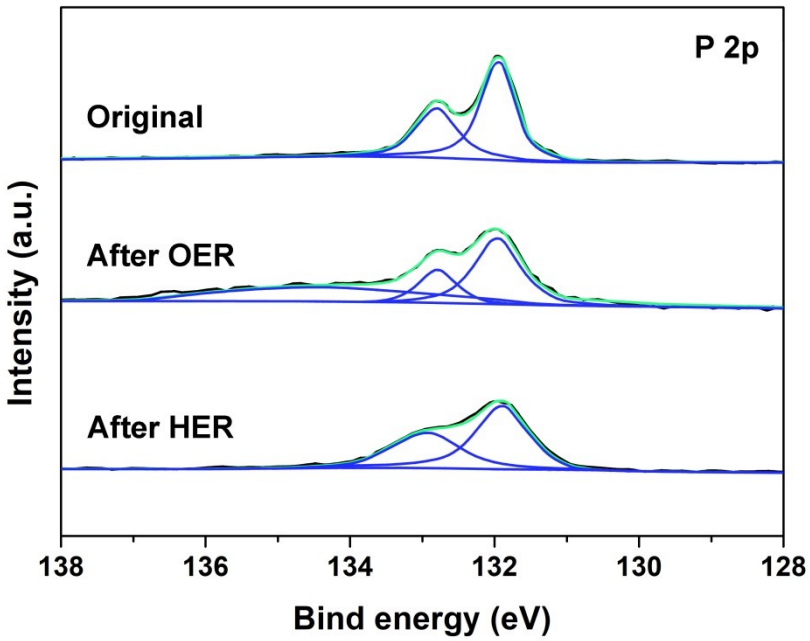

Figure S16. High-resolution XPS spectra for P 2p of SA Co $NiPS_3$ (original, after HER, and after OER).

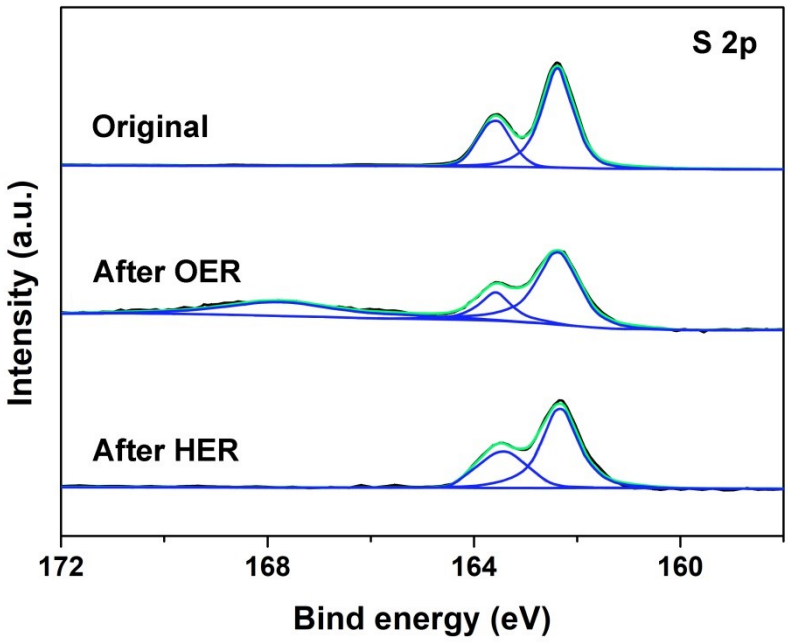

Figure S17. High-resolution XPS spectra for S 2p of SA Co NiPS3 (original, after HER, and after OER).

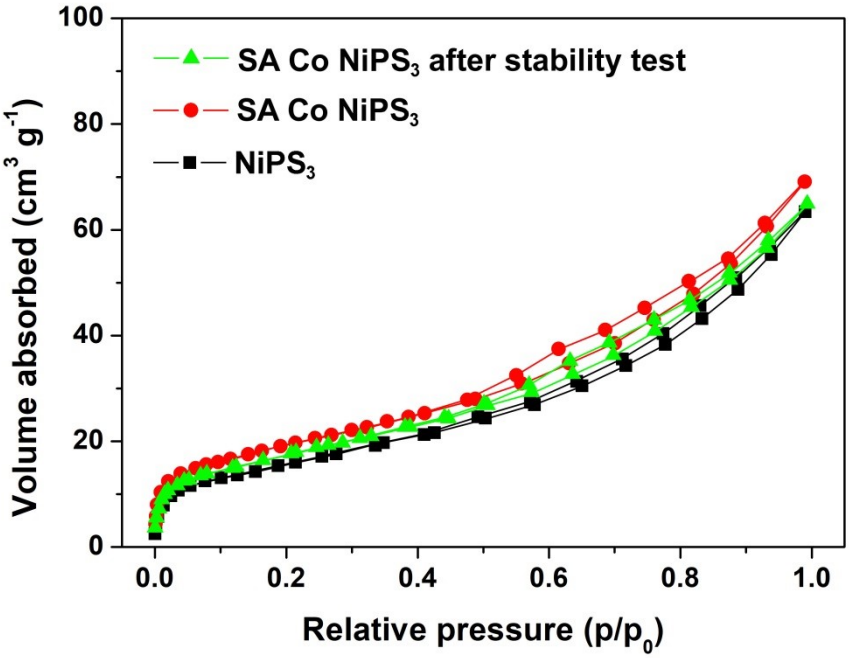

Figure S18. N_2 adsorption-desorption curves of $NiPS_3$, SA Co $NiPS_3$ before and after stability test.

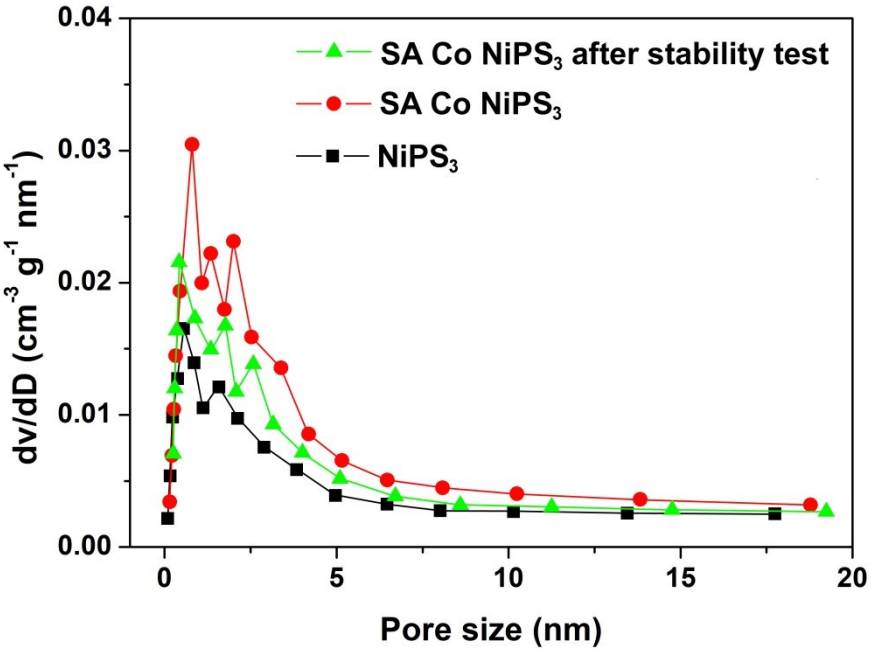

Figure S19. Pore size distributions of $NiPS_3$, SA Co $NiPS_3$ before and after stability test.

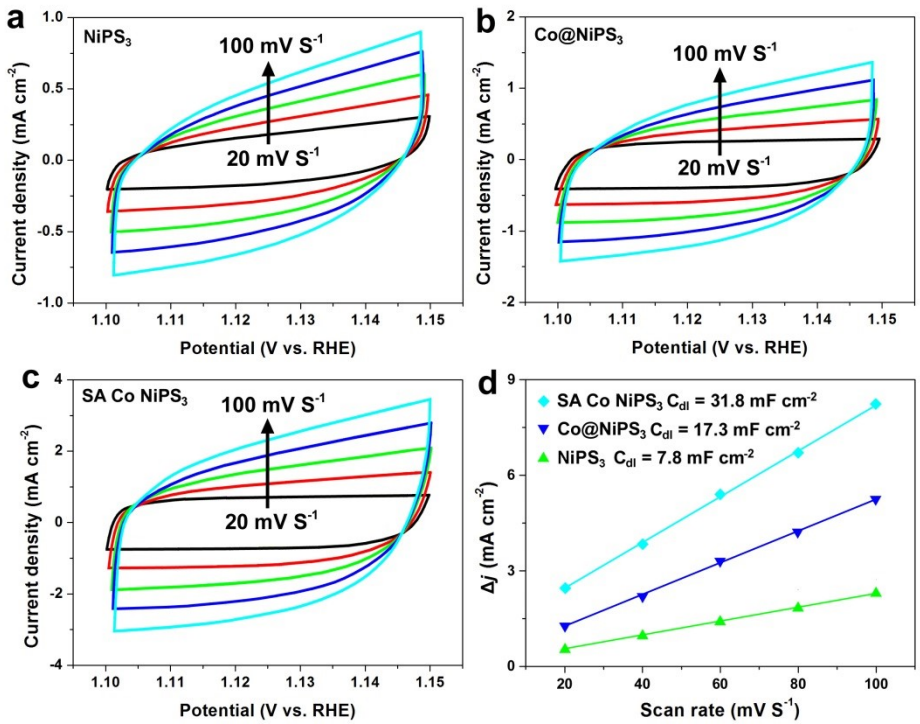

Figure S20. CV curves at 10 mV s^{-1} for (a) $NiPS_3$, (b) Co@$NiPS_3$, and (c) SA Co $NiPS_3$. (d) The changing current density differences (Δj) plotted against scan rates for $NiPS_3$, Co@$NiPS_3$, and SA Co $NiPS_3$.

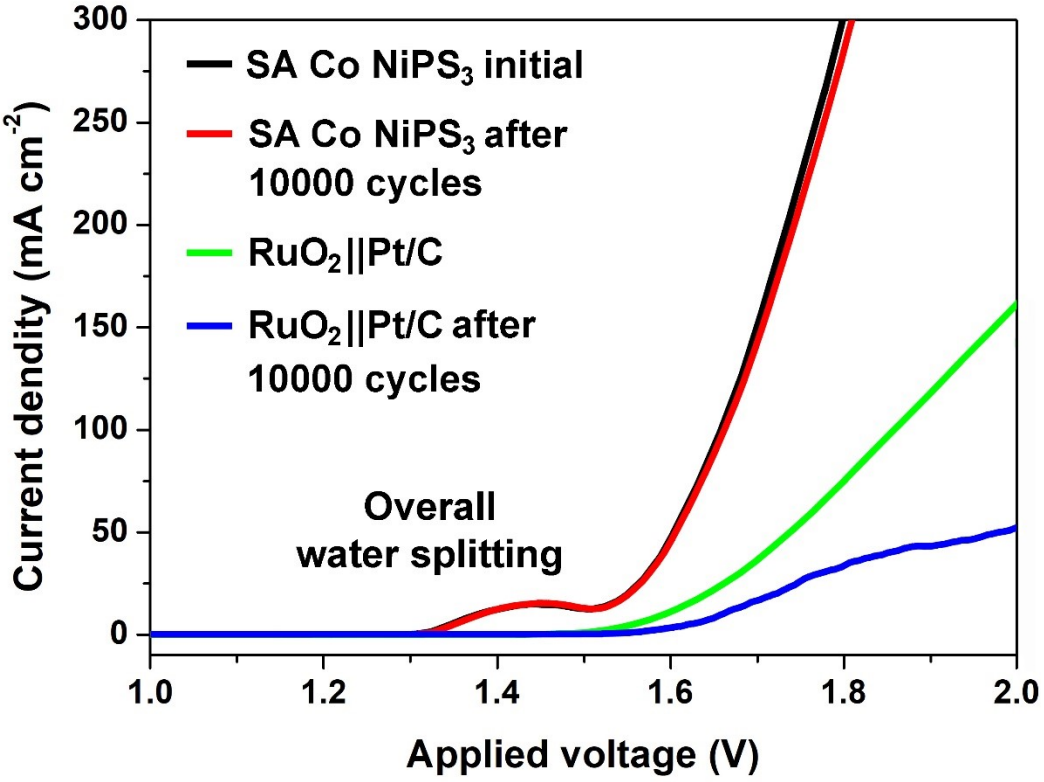

Figure S21. Polarization curves recorded on SA Co $NiPS_3$ before and after 10000 cycles test.

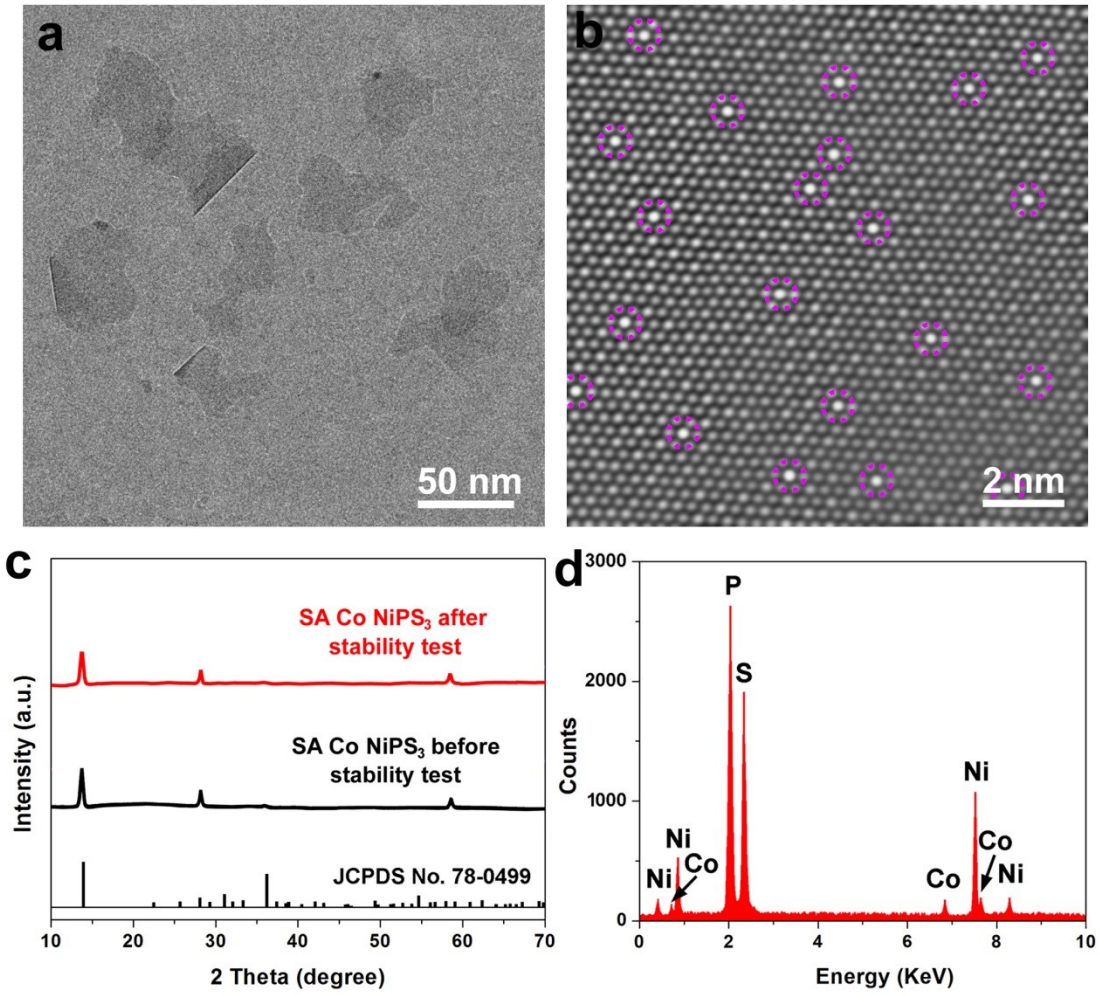

Figure S22. (a) TEM and (b) aberration-corrected HAADF-STEM image of SA Co $NiPS_3$. (c) XRD patterns of SA Co $NiPS_3$ before and after stability test toward water splitting. (d) EDS of SA Co $NiPS_3$ after water splitting stability test.

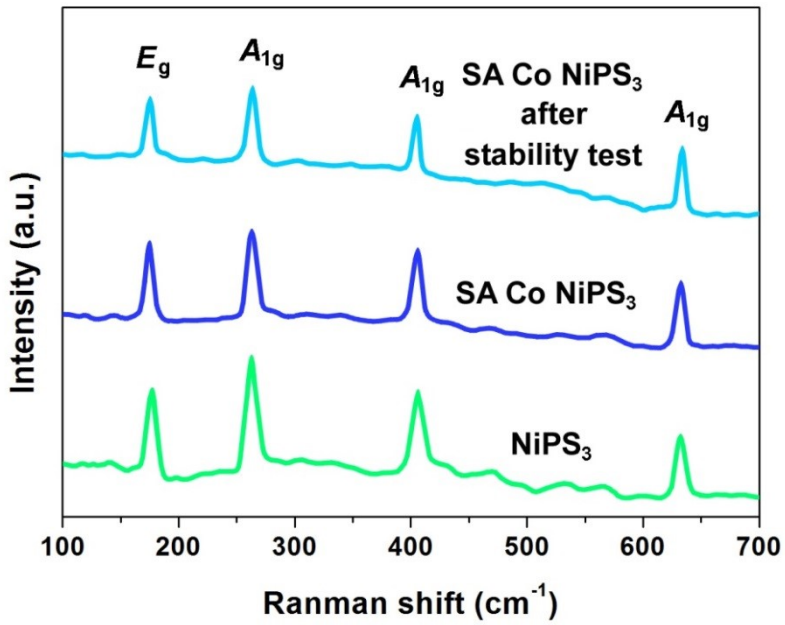

Figure S23. Raman spectra of $NiPS_3$ and SA Co $NiPS_3$ before and after water splitting stability test.

Table S1. Co K-edge EXAFS curve Fitting Parameters obtained from Co@$NiPS_3$ and SA Co $NiPS_3$.

Sample	Bonding	CN	R(Å)	σ^2(×10^{-3}Å^2)	ΔE_0 (eV)	R (%)
Co@$NiPS_3$	Co-Co	7.6	2.501	5.7	6.8	0.12
	Co-S	0.3	2.212	4.7		
SA Co $NiPS_3$	Co-Co	-	-	-	-2.3	0.29
	Co-S	3.4	2.275	9.0		

CN, coordination number; R, distance between absorber and backscatter atoms; σ^2, Debye-Waller factor to account for both thermal and structural disorders; ΔE_0, inner potential correction; R (%) indicates the goodness of the fit. Error bounds (accuracies) that characterize the structural parameters obtained by EXAFS spectroscopy were estimated as N ± 20%; R ± 1%; σ^2 ± 20%; ΔE_0 ± 20%.

Table S2. ICP-AES of the Co@$NiPS_3$ and the SA Co $NiPS_3$.

Sample	Co content / μg	Ni content / μg	Co mass percentage / %
Co@$NiPS_3$	278.5	1279.1	17.82
SA Co $NiPS_3$	32.1	527.3	5.71
SA Co $NiPS_3$ after cycles	37.6	629.1	5.64

Table S3. Comparison of HER performances for SA Co $NiPS_3$ nanosheets with previously reported electrocatalysts in the alkaline media.

Electrocatalyst	Overpotential (mV)	Tafel slope (mV dec-1)	Ref.
SA Co $NiPS_3$	**51, 121 at 10, 50 mA cm^{-2}**	**38.8**	**This Work**
C-doped $NiPS_3$	71 at 10 mA cm^{-2}	38.2	Adv. Funct. Mater. 2020, 30, 1908708
$CoNiPS_3$/C	136 at 30 mA cm^{-2}	60.0	Adv. Funct. Mater. 2018, 28, 1805075
$NiPS_{2.7}Se_{0.3}$	250 at 10 mA cm^{-2}	76.0	Adv. Funct. Mater. 2021, 31, 2100618
$NiPS_3$-G 1:1	294 at 10 mA cm^{-2}	42.0	ACS Nano 2018, 12, 5297.
$NiPS_3/Ni_2P$	85 at 10 mA cm^{-2}	82.0	ACS Nano 2019, 13, 7975-7984
$Co_{2-x}SP$/CFP	279 at 10 mA cm^{-2}	54.0	Adv. Energy Mater. 2018, 8, 1801127.
0.75-Sv-MoS_2	194 at 10 mA cm^{-2}	73.0	Angew, Chem. Int, Ed. 2019, 58, 2029-2033.

MoS_2/NiS_2	50 at 10 mA cm^{-2}	50.1	Adv. Sci. 2019, 6, 1900246
Co,Nb-MoS_2/TiO_2	272 at 10 mA cm^{-2}	40.2	Nano Energy 2021, 82, 105750
Fe doped VOOH	90 at 10 mA cm^{-2}	38.2	Small 2019, 15, 1904688
Mo_3P/Mo	78 at 10 mA cm^{-2}	43.0	Angew. Chem. Int. Ed. 2018, 57, 14139

Table S4. Comparison of OER performances for SA Co $NiPS_3$ nanosheets with previously reported electrocatalysts in the alkaline media.

Electrocatalyst	**Overpotential (mV)**	**Tafel slope (mV dec^{-1})**	**Ref.**
SA Co $NiPS_3$	**1.47 at 50 mA cm^{-2}**	**52.2**	**This Work**
$NiPS_3/Ni_2P$	1.49 at 50 mA cm^{-2}	78.0	ACS Nano 2019, 13, 7975-7984
$NiPS_{2.7}Se_{0.3}$	1.53 at 50 mA cm^{-2}	76.0	Adv. Funct. Mater. 2021, 31, 2100618
MoS_2/NiS_2	3.22 at 10 mA cm^{-2}	91.7	Adv. Sci. 2019, 6, 1900246
Co,Nb-MoS_2/TiO_2	1.59 at 50 mA cm^{-2}	65.0	Nano Energy 2021, 82, 105750
Ni_2P/NF	1.58 at 50 mA cm^{-2}	99.0	Adv. Mater. 2019, 31, 1901174
Mn/Fe-HIB-MOF	2.80 at 10 mA cm^{-2}	45.0	Energy Environ. Sci., 2019, 12, 727
cMOF/LDH array	2.27 at 100 mA cm^{-2}	64.1	Adv. Mater. 2021, 33, 2006351
Ni-Fe LDH DSNC	1.43 at 50 mA cm^{-2}	52	Nano Energy 2021,79, 105418

Table S5. Comparison of overall water splitting performances for SA Co $NiPS_3$ nanosheets with previously reported electrocatalysts in the alkaline media.

Electrocatalyst	Electrolyte	Voltage/30 mA cm^{-2}	Ref.
SA Co $NiPS_3$	**1 M KOH**	**1.57**	**This Work**
$NiPS_3/Ni_2P$	1 M KOH	1.58	ACS Nano 2019, 13, 7975-7984
$CoNiPS_3/C$	1 M KOH	1.51	Adv. Funct. Mater. 2018, 28, 1805075
MoS_2/NiS_2	1 M KOH	1.61	Adv. Sci. 2019, 6, 1900246
$Co,Nb\text{-}MoS_2/TiO_2$	1 M KOH	1.70	Nano Energy 2021, 82, 105750
$G/MoS_2/FeCoNi(OH)_x$	1 M KOH	1.45	Nat. Commun. 2021, 12, 21742
$BiVO_4/Ti_3C_2$	1 M KOH	1.58	Appl. Catal. B: Enviren. 2021, 282, 119584,
MoS_2/NiFe-LDH	1 M KOH	1.67	Nano Lett. 2019, 19, 4518-4526
$Au@AuIr_2$	1 M KOH	1.58	J. Am. Chem. Soc. 2021, 143, 4639-4645
$Ni_2P\text{-}CuP_2$ on Ni- G-CNTs	1 M KOH	1.48	ACS Nano 2021, 15, 5586-5599
$WN\text{-}Ni(OH)_2$	1 M KOH	1.72	ACS Catalysis 2020, 10, 13323-13333
Co_9S_8/Ni_3S_2/NF	1 M KOH	1.67	J. Am. Chem. Soc. 2019, 141, 10417-10430
$NiCo_2S_4$ NW/NF	1 M KOH	1.79	Adv. Funct. Mater.

			2016, 26, 4661-4672

References

[1] Black, C. T., Murry, C. B., Sandstrom, R. L. & Sun, S. H. Spin dependent tunneling in self assembled cobalt nanocrystal superlattices, *Science* **2000**, *290*, 1131-1134.

[2] Y. Du, Y. Zhu, S. Xi, P. Yang, H. Moser, M. Breese, A. Borgna, XAFCA: A new XAFS beamline for catalysis research, *J. Synchrotron Radiat.* **2015**, *22*, 839-843.

[3] B. Ravel, M. Newville, Athena, Artemis, Heohaestus: data analysis for X-ray absorption spectroscopy using IFEFFIT, *J. Synchrotron Radiat.* **2005**, *12*, 537-541.

[4] G. Kresse, J. Furthmuller, Efficient iterative schemes for ab initio total-energy calculations using a plane-wave basis set, *Phys. Rev. B* **1996**, *54*, 11169-11186.

[5] J. Perdew, J. Chevary, S. Vosko, K. Jackson, M. Pederson, D. Singh C. Fiolhais, Atoms, molecules, solids and surfaces: applications of the generalized gradient approximation for exchange and correlation, *Phys. Rev. B* **1992**, *46*, 6671-6687.

[6] P. Blochl, Projector augmented-wave method, *Phys. Rev. B* **1994**, *50*, 17953-17979.

[7] J. Wang, X. Li, B. Wei, R. Sun, W. Yu, H. Hoh, H. Xu, J. Li, X. Ge, Z. Chen, C. Su, Z. Wang, Activating basal planes of $NiPS_3$ for hydrogen evolution by nonmetal heteroatom doping, *Adv. Funct. Mater.* **2020**, *30*, 1908708.